PHYSICAL REVIEW
LETTERS

VOLUME 59 13 JULY 1987 NUMBER 2

Scaling Structure of Attractors at the Transition from Quasiperiodicity to Chaos in Electronic Transport in Ge

E. G. Gwinn and R. M. Westervelt
Division of Applied Sciences and Department of Physics, Harvard University, Cambridge, Massachusetts 02138
(Received 26 March 1987)

We present a high-precision experimental verification of the universality of $f(\alpha)$, the fractal dimension of the subset of the attractor with scaling index α, at the transition from quasiperiodicity to chaos with the golden-mean winding number. The experimental system is cooled extrinsic p-type Ge, which is voltage biased to produce a spatially dependent active oscillation.

PACS numbers: 05.45.+b, 72.20.Ht, 72.70.+m

Attractors for typical dynamical systems can be described as the union of many interwoven fractal sets.[1-5] Each set is characterized by an index α which describes how the total probability contained in a small region surrounding an element of the set scales with the size of the region. The function $f(\alpha)$ is the fractal dimension of the set with index α, and is expected to be universal for systems with other universal scaling properties; for example, driven nonlinear oscillators at the transition from quasiperiodicity to chaos with winding number equal to the golden mean.

Universal predictions of circle-map theory[6-9] for structure in the Arnold tongue diagram and in the power spectrum at the transition from quasiperiodicity to chaos have been tested in experiments on several different driven nonlinear oscillator systems.[10-15] Agreement between theory and experiment was first obtained by Fein, Heutmaker, and Gollub[10] for fluid convection. Subsequent work[11-15] by other groups has achieved excellent quantitative agreement between circle-map theory and experiment. However, experimental confirmation of the universality of $f(\alpha)$ has been sparse, in part because of the noise sensitivity[16] of this quantity: A series of fluid-convection experiments[3,17] have provided the only published confirmation of theory. In this Letter we present a high-precision experimental confirmation of the universality of $f(\alpha)$ at the transition from quasiperiodicity to chaos for a spatially dependent transport instability in cooled p-type Ge.

The experimental details have been described previously in a test of the universal power spectrum.[15] The sample is a $4\times8\times8$-mm^3 crystal of p-type Ge with acceptor concentration $a\cong1\times10^{11}$ cm^{-3}, and has B-ion-implanted p^+ contacts which cover both parallel 8×8-mm^2 faces. These contacts act as ideal reservoirs for holes at 4 K and were able to supply >10 mA of current without introducing excess noise. The Ge sample was mounted in vacuum on a cold plate enclosed in two concentric cooled radiation shields, and cooled to temperatures $T\cong4$ K. The sample was dc voltage biased above the threshold by 5 V/cm for impact ionization of shallow acceptor levels, where the dc I-V characteristic has a region of voltage-controlled (N-type) negative differential resistance. This type of I-V characteristic can be generally shown to produce oscillatory spatial structure in the form of planar electric field domains.[18-20] The time-dependent current oscillation produced by this instability in Ge has a very stable frequency, and a signal-to-noise ratio greater than the 80-dB dynamic range of the Hewlett-Packard model 3561A signal analyzer used to record data.

In order to drive the sample to the transition from quasiperiodicity to chaos, we superimposed sinusoidal and dc voltages of amplitudes V_{ac} and V_{dc}, respectively, with V_{dc} fixed at 3.05 V, where the spontaneous oscillation frequency has a minimum at $f_0=8020$ Hz. The frequency of the sinusoidal voltage bias was adjusted so that the ratio of the response frequency to the drive fre-

quency was within three parts in 10^5 of the golden mean $\sigma_g=(5^{1/2}-1)/2$. The amplitude V_{ac} for the transition to chaos at σ_g was determined experimentally as the amplitude $V_{ac}=153$ mV which gave the best agreement between the measured current power spectrum $S(f)$ and the spectrum predicted by circle-map theory.[9,15] This was done by our computing and displaying the normalized current power spectrum in real time as V_{ac} was adjusted to produce the maximum number of peaks with characteristic self-similar structure between frequency intervals differing by factors of the golden mean.[15] With the drive frequency and amplitude adjusted to these values, Poincaré sections of the attractor were measured as time series by recording of the sample current $I(t)$ once per drive cycle, at constant drive phase, using the Hewlett-Packard model 3561A signal analyzer in external-sample mode. We typically recorded five series of 42960 contiguous current samples each onto the hard disk of a microcomputer attached to the signal analyzer.

Figure 1 shows a Poincaré section of the attractor at the onset of chaos with winding number σ_g, reconstructed from the current time series $I(t)$. To calculate $f(\alpha)$ for a set such as Fig. 1, one must choose a measure of the distance between points on the Poincaré section. Two obvious choices are the Euclidean distance in the embedding space, and the distance measured along the Poincaré section itself. For small length scales, these distances are nearly identical, but for lengths approaching the size of the attractor, the bends and curves in the Poincaré section cause them to differ. In order to maximize the range of length scales over which the scaling is good, we measured distances along the Poincaré section itself. This was accomplished by use of a ridge-finding algorithm to locate a high-probability path around the Poincaré section. A time series with one spatial coordinate was constructed by moving each datum point in the original section to the nearest point on the ridge, which closely follows the Poincaré section of Fig. 1. The distance between trajectory points is measured as the path length s along the ridge, with the total distance around the section normalized to 1. This measure of the distance was found to give the same correlation dimension[4] D_2 as the Euclidean distance in two- and three-dimensional embeddings, but yielded the best scaling of these three techniques, as discussed below.

Figure 2 shows a histogram of the probability density on the Poincaré section of Fig. 1, measured along the length of the section in units of s. As shown, the distribution is highly singular, and is similar to the probability density determined from the circle map at the onset of chaos. Such a distribution can be decomposed into a continuum of fractal sets, each with a scaling index[3-5] α which describes how the probability $p_s(L)$ contained within a region of size L about a member of the set located at s scales with L. We determine this probability directly from

$$p_s(L)=N_s(L)/N_{tot}, \tag{1}$$

where $N_s(L)$ is the number of points from a long trajectory of N_{tot} points which fall within a distance L of the point at s. For small L, $p_s(L)\propto L^{\alpha}$; this relationship defines[3-5] the scaling index α. The elements of a set with a particular value of α are distributed over the attractor, and form a structure with fractal (Hausdorff) dimension $f(\alpha)$. Small values of α are associated with parts of the attractor where the probability is very concentrated; for example, the sharply peaked regions of Fig. 2. Large values of α correspond to regions of the attractor that are rarely visited, such as the deep valleys in Fig. 2. By calculating $p_s(L)$ directly from Eq. (1), using long data sets, we avoided the recurrence-time approximation required by short data sets in previous experi-

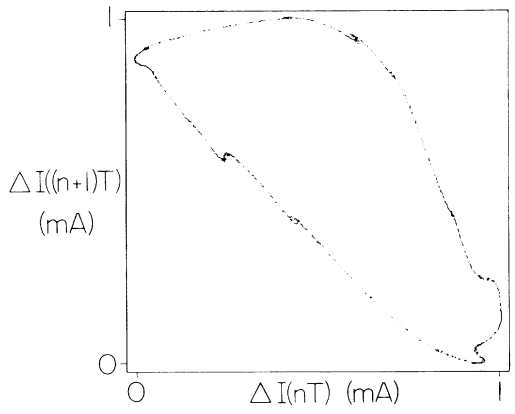

FIG. 1. Experimental Poincaré section reconstructed from the current time series $I(t)=I_0+\Delta I(t)$ at the transition from quasiperiodicity to chaos with golden-mean winding number, where $I_0\cong 5$ mA; n and T are the number and period of drive cycles.

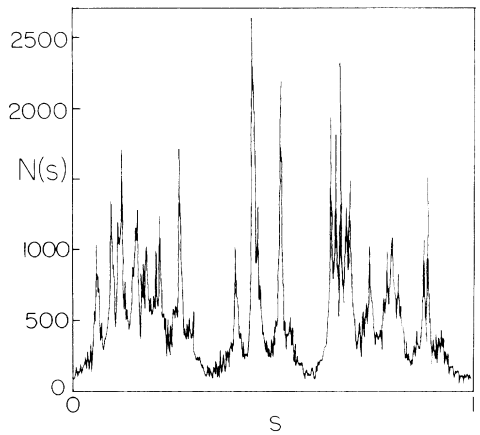

FIG. 2. Histogram of the probability density on the Poincaré section of Fig. 1, with the spatial coordinate s measured along the section itself.

mental work.[3,17] For the smallest experimental length scales, $L=5\times10^{-3}$, and the most sparsely visited regions of the attractor, a trajectory of approximately 5×10^4 elements was required to achieve 10% accuracy in $p_s(L)$.

The spectrum $f(\alpha)$ can be found[3-5] from a generating function $\Gamma(q,L)$:

$$\Gamma(q,L)=\langle p_s(L)^{q-1}\rangle, \tag{2}$$

where the average is over consecutive elements of a trajectory on the attractor. The quantity q selects the value of α which dominates the average in Eq. (2); for large positive q, peaks in the probability distribution corresponding to small values of α dominate $\Gamma(q,L)$, and for large negative q, valleys corresponding to large values of α are heavily weighted. We calculated $\Gamma(q,L)$ from our data using Eq. (2) with 5000 values of $p_s(L)$.

For small length scales L, $\Gamma(q,L)$ is found to scale with L according to the power law[3-5]

$$\Gamma(q,L)\propto L^{\tau(q)}. \tag{3}$$

The quantities α and $f(\alpha)$ can be calculated from $\tau(q)$ by use of[3-5]

$$\alpha=d\tau(q)/dq, \tag{4a}$$

$$f(\alpha)=q\,d\tau/dq-\tau(q). \tag{4b}$$

In practice, experimental noise introduces a lower length-scale cutoff[16] to Eq. (3). Because compression in the phase space onto the attractor is strong, and because trajectories begin to diverge along the Poincaré section at the onset of chaos, small levels of experimental noise are amplified along the Poincaré section to produce approximately one-dimensional scaling in the range $L_d<L<L_1$, where L_d and L_1 are the noise-induced excursions perpendicular and parallel to the section. Over this range, $p_s(L)\propto L^{\alpha}$, with $\alpha\cong1$, and consequently the noise-induced slope $\tau_n(q)\cong q-1$, from Eqs. (2) and (3). For length scales $L<L_d$, the probability $p_s(L)$ should grow as L^d, where d is the dimension of the embedding. The range of experimental length scales that gives universal scaling lies between L_1, which varies rapidly[16] with q, and $L=1$, the size of the attractor.

Figure 3 shows several examples of the log-log plots of $\Gamma(q,L)$ vs L used to determine $\tau(q)$ and thereby $f(\alpha)$ from experimental data. These illustrate both the method of analysis and the problems imposed by its sensitivity to noise. As shown, $\Gamma(q,L)$ is dominated by the effects of noise for negative q and small L: The slope $\tau_n=d\log[\Gamma(q,L)]/d\log(L)\cong q-1$ for the smallest L is just that predicted above for noise. For larger L a break in slope occurs at L_1, above which $\Gamma(q,L)$ accurately scales with L as $\tau(q)$ predicted by the universal theory. As illustrated in Fig. 3, the upper length-scale cutoff of the universal scaling region moves to smaller L for large positive and negative q, because more isolated regions of the attractor dominate $\Gamma(q,L)$ in either case. These constraints limit the range of q for which $\tau(q)$ is easily evaluated to roughly $-3\le q\le6$. We found that the recurrence-time estimate[3] required for smaller data sets with $\simeq4000$ points produces rounded steps in $\Gamma(q,L)$. These steps make the noise scaling for small L unobservable, and prevent an accurate determination of the universal scaling region. These problems occur for circle-map time series as well as for our experimental data. Thus the limitations imposed on experimental measurements of $f(\alpha)$ are severe: Both high signal-to-noise levels and large data sets are required.

We measured $\tau(q)$ and $f(\alpha)$ as described above from three experimental data sets of $\simeq7\times10^4$ data points each, recorded at the critical amplitude $V_{ac}=153$ mV with the experimental winding number adjusted to the golden mean. The average of these experimental results for $f(\alpha)$ is shown in Fig. 4 together with the universal $f(\alpha)$ curve computed in the same way from the sine cir-

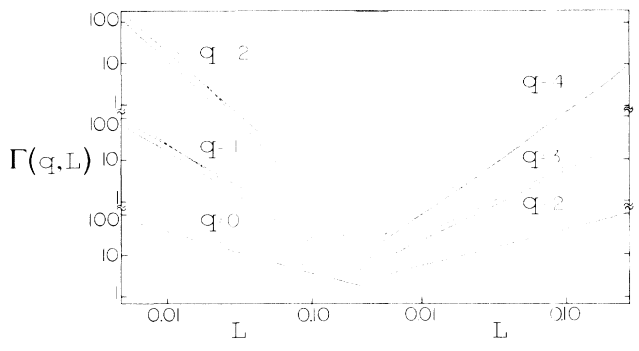

FIG. 3. Log-log plots of $\Gamma(q,L)$ vs L for several values of q, as indicated. The dashed lines for negative q and small L indicate the predicted noise slope $\tau_n(q)$; the slope of the dashed lines for intermediate L show the measured $\tau(q)$.

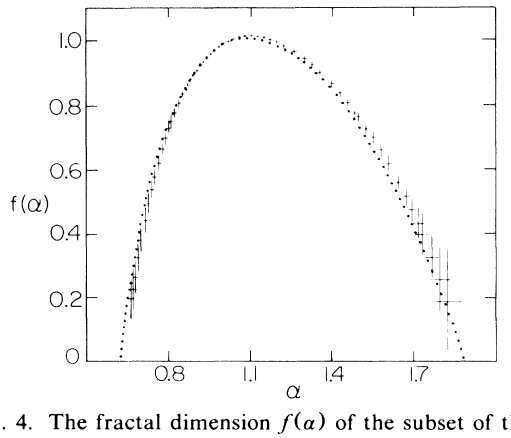

FIG. 4. The fractal dimension $f(\alpha)$ of the subset of the experimental attractor with scaling index α, shown with error bars indicating the standard deviation of the mean of three data sets. The universal circle map result is shown as a dotted curve for comparison.

cle map.[9] The experimental error bars shown in Fig. 4 are simply the standard deviation of the mean of the three data sets. As shown, the experimental results for $f(\alpha)$ are in striking agreement with universal theory; this comparison is made with no adjustable parameters. The overall level of agreement shown in Fig. 4 is roughly a factor of 4 better than obtained previously. This agreement is physical evidence for the relevance of circle map theory to our experimental system, which has both spatial and temporal degrees of freedom, and which is in principal infinite-dimensional.

The largest errors in our experiment are caused by sensitivity to the ratio of the drive and response frequencies and to the drive amplitude: A change in drive amplitude V_{ac} of 1% causes a noticeable narrowing of the $f(\alpha)$ curve.[21] In addition, the techniques used to analyze the data are sensitive to noise as discussed above. The width of the universal scaling region for $\Gamma(q,L)$ decreases fairly rapidly with increasing noise level and $|q|$, and for sufficiently large noise level or $|q|$, the universal power law $\Gamma(q,L) \propto L^{\tau(q)}$ will not be observed at *any* length scale. This noise sensitivity presents difficulties in the use of $f(\alpha)$ to characterize the attractors of typical experimental systems.

We thank L. Kadanoff, M. Jensen, and K. L. Babcock for helpful discussions. One of us (E.G.G.) acknowledges support as an AT&T Bell Laboratories Scholar. This work was supported in part by the U.S. Office of Naval Research under Contract No. N00014-84-K-0329.

[1]H. G. E. Hentschel and I. Procaccia, Physica (Amsterdam) **8D**, 435 (1983).

[2]R. Benzi, G. Paladin, G. Parisi, and A. Vulpiani, J. Phys. A **17**, 3521 (1984).

[3]M. H. Jensen, L. P. Kadanoff, A. Libchaber, I. Procaccia, and J. Stavans, Phys. Rev. Lett. **55**, 2798 (1985).

[4]T. C. Halsey, M. H. Jensen, L. P. Kadanoff, I. Procaccia, and B. I. Shraiman, Phys. Rev. A **33**, 1141 (1986).

[5]T. C. Halsey and M. H. Jensen, Physica (Amsterdam) **5D**, 112 (1986).

[6]M. J. Feigenbaum, L. P. Kadanoff, and S. J. Shenker, Physica (Amsterdam) **5D**, 370 (1982).

[7]D. Rand, S. Ostlund, J. Sethna, and E. D. Siggia, Phys. Rev. Lett. **49**, 132 (1982).

[8]S. J. Shenker, Physica (Amsterdam) **5D**, 405 (1982).

[9]S. Ostlund, D. Rand, J. Sethna, and E. Siggia, Physica (Amsterdam) **8D**, 303 (1983).

[10]A. P. Fein, M. S. Heutmaker, and J. P. Gollub, Phys. Scr. **T9**, 79 (1985).

[11]J. Stavans, F. Heslot, and A. Libchaber, Phys. Rev. Lett. **55**, 596 (1985).

[12]H. L. Swinney and J. Maselko, Phys. Rev. Lett. **55**, 2366 (1985).

[13]G. A. Held and C. Jeffries, Phys. Rev. Lett. **56**, 1183 (1986).

[14]S. Martin and W. Martienssen, Phys. Rev. Lett. **56**, 1522 (1986).

[15]E. G. Gwinn and R. M. Westervelt, Phys. Rev. Lett. **57**, 1060 (1986), and **59**, 247(E) (1987) (this issue).

[16]E. G. Gwinn and R. M. Westervelt, to be published.

[17]J. A. Glazier, M. H. Jensen, A. Libchaber, and J. Stavans, Phys. Rev. A **34**, 1621 (1986).

[18]K. Seeger, *Semiconductor Physics* (Springer-Verlag, New York, 1982).

[19]S. W. Teitsworth and R. M. Westervelt, Physica (Amsterdam) **23D**, 181 (1986).

[20]S. W. Teitsworth, Ph.D. thesis, University Microfilms International, Ann Arbor, 1986 (unpublished).

[21]In principle $f(\alpha)$ very rapidly narrows to a point below the critical amplitude when determined on arbitrarily small length scales, as discussed by A. Arneodo and M. Holschneider, Phys. Rev. Lett. **58**, 2007 (1987). However, on larger length scales which are experimentally accessible, the apparent $f(\alpha)$ changes much less rapidly. For the sine circle map, the width of $f(\alpha)$ determined by the algorithm used here (see Refs. 3–5) narrows by 7% at an amplitude 1% below the critical line.